Physics Letters B 845 (2023) 138164

Contents lists available at ScienceDirect

Physics Letters B

journal homepage: www.elsevier.com/locate/physletb

Direct tests of T, CP, CPT symmetries in transitions of neutral K mesons with the KLOE experiment

The KLOE-2 Collaboration

D. Babusci [c], M. Berłowski [r], C. Bloise [c], F. Bossi [c], P. Branchini [n], B. Cao [o], F. Ceradini [m,n], P. Ciambrone [c], F. Curciarello [h,i], E. Czerwiński [b,*], G. D'Agostini [k,l], R. D'Amico [k,l], E. Danè [c], V. De Leo [k,l], E. De Lucia [c], A. De Santis [c], P. De Simone [c], A. Di Domenico [k,l], E. Diociaiuti [c], D. Domenici [c], A. D'Uffizi [c], G. Fantini [k,l], A. Gajos [b], S. Gamrat [b], P. Gauzzi [k,l], S. Giovannella [c], E. Graziani [n], X. Kang [q], A. Kupść [o,r], G. Mandaglio [e,a], M. Martini [c,j], S. Miscetti [c], P. Moskal [b], A. Passeri [n], E. Pérez del Río [b], M. Schioppa [h,i], A. Selce [m,n], M. Silarski [b], F. Sirghi [c,d], E.P. Solodov [f,g], W. Wiślicki [r], M. Wolke [o], J. Bernabéu [p]

[a] *INFN Sezione di Catania, Catania, Italy*
[b] *Institute of Physics, Jagiellonian University, Cracow, Poland*
[c] *Laboratori Nazionali di Frascati dell'INFN, Frascati, Italy*
[d] *Horia Hulubei National Institute of Physics and Nuclear Engineering, Măgurele, Romania*
[e] *Dipartimento di Scienze Matematiche e Informatiche, Scienze Fisiche e Scienze della Terra dell'Università di Messina, Messina, Italy*
[f] *Budker Institute of Nuclear Physics, Novosibirsk, Russia*
[g] *Novosibirsk State University, Novosibirsk, Russia*
[h] *Dipartimento di Fisica dell'Università della Calabria, Arcavacata di Rende, Italy*
[i] *INFN Gruppo collegato di Cosenza, Arcavacata di Rende, Italy*
[j] *Dipartimento di Scienze e Tecnologie applicate, Università "Guglielmo Marconi", Roma, Italy*
[k] *Dipartimento di Fisica dell'Università "Sapienza", Roma, Italy*
[l] *INFN Sezione di Roma, Roma, Italy*
[m] *Dipartimento di Matematica e Fisica dell'Università "Roma Tre", Roma, Italy*
[n] *INFN Sezione di Roma Tre, Roma, Italy*
[o] *Department of Physics and Astronomy, Uppsala University, Uppsala, Sweden*
[p] *Department of Theoretical Physics, University of Valencia, and IFIC, Univ. Valencia-CSIC, E-46100 Burjassot, Valencia, Spain*
[q] *School of Mathematics and Physics, China University of Geosciences (Wuhan), Wuhan, China*
[r] *National Centre for Nuclear Research, Warsaw, Poland*

ARTICLE INFO

Article history:
Received 8 December 2022
Received in revised form 27 July 2023
Accepted 29 August 2023
Available online 4 September 2023
Editor: M. Pierini

Keywords:
Discrete and finite symmetries
Kaon physics
CP violation

ABSTRACT

Tests of the T, CP and CPT symmetries in the neutral kaon system are performed by the direct comparison of the probabilities of a kaon transition process to its symmetry-conjugate. The exchange of *in* and *out* states required for a genuine test involving an antiunitary transformation implied by time-reversal is implemented exploiting the entanglement of $K^0\overline{K}^0$ pairs produced at a ϕ-factory.

A data sample collected by the KLOE experiment at DAΦNE corresponding to an integrated luminosity of about 1.7 fb^{-1} is analysed to study the Δt distributions of the $\phi \to K_S K_L \to \pi^+\pi^-\pi^\pm e^\mp \nu$ and $\phi \to K_S K_L \to \pi^\pm e^\mp \nu 3\pi^0$ processes, with Δt the difference of the kaon decay times. A comparison of the measured Δt distributions in the asymptotic region $\Delta t \gg \tau_S$ allows to test for the first time T and CPT symmetries in kaon transitions with a precision of few percent, and to observe CP violation with this novel method.

1. Introduction

Symmetries and their breaking in the physical laws play a crucial role in fundamental physics and other fields. Besides local gauge symmetries generated by charges the discrete symmetries

* Corresponding author.
E-mail address: eryk.czerwinski@uj.edu.pl (E. Czerwiński).

https://doi.org/10.1016/j.physletb.2023.138164

are also of maximal relevance. The breaking of Parity – P, Charge Conjugation – C, and the combined CP symmetries has oriented the understanding of the electroweak and flavour sectors of particle physics. Whereas P, C and CP are implemented by unitary operators, Time Reversal – T and CPT transformations are antiunitary [1]. This fact implies that, besides the transformation of initial and final states in a given process, the two states have to be exchanged for a genuine direct test of the symmetry. For unstable particles this requirement, being the decay irreversible for all practical purposes, seems to lead to a *no-go* argument [2,3]. The latter can be bypassed considering that the *reversal-in-time* does not include the decay products, but only the *motion-reversal* before the decay, the decay being instrumental for tagging the initial meson state and filtering the final state [4,5]. This is made possible by exploiting the maximal entanglement of meson–antimeson pairs, as $B^0\overline{B}^0$ produced at B-factories, or $K^0\overline{K}^0$ produced at ϕ-factories. This conceptual basis for the search of Time Reversal Violation (TRV) effects was immediately recognised [2] as being a genuine test. The methodology for the entire procedure was developed in Ref. [6] for the B^0-system, yielding the first direct observation of TRV by the BABAR Collaboration [7] (additional information can be found in Refs. [8,9]). For the K-system, the methodology for the test in transitions involving meson decays into specific flavour or CP final states was described in Refs. [10,11].

For the $K^0 - \overline{K}^0$ system, the CPLEAR Collaboration obtained a 4σ evidence of the asymmetry between the process $K^0 \to \overline{K}^0$ and its inverse $\overline{K}^0 \to K^0$ [12]. However, its interpretation in terms of a genuine TRV effect is controversial, raising some issues [2,3,13] related to the decay as essential ingredient. In fact, an initial state absorptive interaction between K^0 and $\overline{K}^0$ is needed to generate the TRV effect in this case, leading to an asymmetry constant in time, due to the non-orthogonality of K_L and K_S. Moreover, for the $K^0 \to \overline{K}^0$ transition its CPT transformed is the identity, not distinguishing T and CP conjugate transitions, even if CPT is violated. The related CPT test performed by CPLEAR is based on the comparison of the $K^0 \to K^0$ and $\overline{K}^0 \to \overline{K}^0$ processes, i.e. the K^0 and $\overline{K}^0$ survival probabilities [14].

In this letter we present the results of the first direct T, CP, CPT tests performed in the $K^0 - \overline{K}^0$ system, obtained analysing the data collected by the KLOE experiment at the DAΦNE ϕ-factory, and according to the methodology described in Refs. [10,11]. The transitions involved are those between the states tagged and filtered by the CP and flavour eigenstate decay products. In different combinations, they allow to build direct, genuine and separate observables for T, CP and CPT asymmetries. In particular, the test based on the measurement of a double CPT ratio is very clean, free from approximations and model independent, and constitutes an excellent tool to advance the search for CPT violation. In fact, CPT invariance has a very solid theoretical justification in the CPT theorem [15–18], valid for quantum field theories satisfying Lorentz invariance, local interaction and unitarity, and an unambiguous observation of its violation would have grave consequences for our understanding of particle physics. Probing CPT in transitions selects a different sensitivity to violating effects with respect to the test [14] based on survival probabilities for K^0 and $\overline{K}^0$ involving diagonal terms of the Hamiltonian.

2. Transition probabilities and double decay intensities

In order to implement the T, CP and CPT tests, the entanglement of neutral kaons produced at DAΦNE (see recent experimental [19] and theoretical studies [20] on this subject) is exploited. In fact, in this case the initial state of the neutral kaon pair produced in $\phi \to K^0\overline{K}^0$ decay can be rewritten in terms of any pair of orthogonal states $|K_+\rangle$ and $|K_-\rangle$ as:

$$|i\rangle = \frac{1}{\sqrt{2}}\{|K^0\rangle|\overline{K}^0\rangle - |\overline{K}^0\rangle|K^0\rangle\} = \frac{1}{\sqrt{2}}\{|K_+\rangle|K_-\rangle - |K_-\rangle|K_+\rangle\} \ . \quad (1)$$

In order to formulate the test, it is necessary to precisely define the different states involved as *in* and *out* states in the considered transition process. First, let us consider the states $|K_-\rangle$, $|K_+\rangle$ defined as follows: $|K_-\rangle$, $|K_+\rangle$ are the states tagged by the observation of the partner decay into the $CP = +, -$ eigenstate decay products $\pi^+\pi^-$ (or equivalently $\pi^0\pi^0$) and $3\pi^0$,[1] respectively. They are explicitly identified as the states not decaying to these channels:

$$\begin{aligned} |K_-\rangle &\propto |K_L\rangle - \eta_{+-}|K_S\rangle \\ |K_+\rangle &\propto |K_S\rangle - \eta_{000}|K_L\rangle \ , \end{aligned} \quad (2)$$

with $\eta_{+-} = \langle\pi^+\pi^-|\mathcal{T}|K_L\rangle/\langle\pi^+\pi^-|\mathcal{T}|K_S\rangle$ and $\eta_{000} = \langle 3\pi^0|\mathcal{T}|K_S\rangle/\langle 3\pi^0|\mathcal{T}|K_L\rangle$. Thus their orthogonal states $|K^\perp_-\rangle$, $|K^\perp_+\rangle$ are those filtered by their observed decays. The orthogonality condition $|K^\perp_\mp\rangle \equiv |K_\pm\rangle$ corresponds to the assumption of negligible direct CP (and CPT) violation contributions, an assumption well satisfied for neutral kaons in general, and fully satisfied for the specific observables we are going to discuss in the following [11]. As a second orthogonal basis we consider the two flavour eigenstates $|K^0\rangle$ and $|\overline{K}^0\rangle$. The validity of the $\Delta S = \Delta Q$ rule is also assumed [21], so that these states are identified by the charge of the lepton in semileptonic decays, i.e. a $|K^0\rangle$ can decay into $\pi^-e^+\nu$ (or $\pi^-\mu^+\nu$) and not into $\pi^+e^-\overline{\nu}$ (or $\pi^+\mu^-\overline{\nu}$), and vice versa for a $|\overline{K}^0\rangle$.

Thus, exploiting the perfect anticorrelation of the states implied by Eq. (1), it is possible to have a "flavour-tag"or a "CP-tag", i.e. to infer the flavour (K^0 or $\overline{K}^0$) or the CP (K_+ or K_-) state of the still alive kaon by observing a specific flavour decay ($\pi^-e^+\nu$ or $\pi^+e^-\overline{\nu}$) or CP decay ($\pi^+\pi^-$ or $\pi^0\pi^0\pi^0$) of the other (and first decaying) kaon in the pair.

In this way one can experimentally access – for instance – the transition $K^0 \to K_+$, taken as reference, and $K_+ \to K^0$, $\overline{K}^0 \to K_+$ and $K_+ \to \overline{K}^0$, i.e. the T, CP and CPT conjugated transitions, respectively. All possible transitions can be divided into four categories of events, corresponding to independent T, CP and CPT tests. One can directly compare the probabilities for the reference transition and the conjugated transition defining the following ratios of probabilities as a function of the evolution time Δt of the initial kaon state at $\Delta t = 0$ for the T test:

$$\begin{aligned} R_{1,T}(\Delta t) &= P\left[K_+(0) \to \overline{K}^0(\Delta t)\right] / P\left[\overline{K}^0(0) \to K_+(\Delta t)\right] \\ R_{2,T}(\Delta t) &= P\left[K^0(0) \to K_-(\Delta t)\right] / P\left[K_-(0) \to K^0(\Delta t)\right] \\ R_{3,T}(\Delta t) &= P\left[K_+(0) \to K^0(\Delta t)\right] / P\left[K^0(0) \to K_+(\Delta t)\right] \\ R_{4,T}(\Delta t) &= P\left[\overline{K}^0(0) \to K_-(\Delta t)\right] / P\left[K_-(0) \to \overline{K}^0(\Delta t)\right] \ , \end{aligned} \quad (3)$$

for the CP test:

$$\begin{aligned} R_{1,CP}(\Delta t) &= P\left[K_+(0) \to \overline{K}^0(\Delta t)\right] / P\left[K_+(0) \to K^0(\Delta t)\right] \\ R_{2,CP}(\Delta t) &= P\left[K^0(0) \to K_-(\Delta t)\right] / P\left[\overline{K}^0(0) \to K_-(\Delta t)\right] \\ R_{3,CP}(\Delta t) &= P\left[\overline{K}^0(0) \to K_+(\Delta t)\right] / P\left[K^0(0) \to K_+(\Delta t)\right] \\ R_{4,CP}(\Delta t) &= P\left[K_-(0) \to K^0(\Delta t)\right] / P\left[K_-(0) \to \overline{K}^0(\Delta t)\right] \ , \end{aligned} \quad (4)$$

or for the CPT test:

[1] The $\pi^+\pi^-\pi^0$ final state, even though dominated by the S-wave contribution, is not a pure $CP = -1$ state, and is therefore not appropriate for precision tests of discrete symmetries.

$$R_{1,\mathrm{CPT}}(\Delta t) = P\left[\mathrm{K}_+(0) \to \overline{\mathrm{K}}^0(\Delta t)\right] / P\left[\mathrm{K}^0(0) \to \mathrm{K}_+(\Delta t)\right]$$
$$R_{2,\mathrm{CPT}}(\Delta t) = P\left[\mathrm{K}^0(0) \to \mathrm{K}_-(\Delta t)\right] / P\left[\mathrm{K}_-(0) \to \overline{\mathrm{K}}^0(\Delta t)\right]$$
$$R_{3,\mathrm{CPT}}(\Delta t) = P\left[\mathrm{K}_+(0) \to \mathrm{K}^0(\Delta t)\right] / P\left[\overline{\mathrm{K}}^0(0) \to \mathrm{K}_+(\Delta t)\right]$$
$$R_{4,\mathrm{CPT}}(\Delta t) = P\left[\overline{\mathrm{K}}^0(0) \to \mathrm{K}_-(\Delta t)\right] / P\left[\mathrm{K}_-(0) \to \mathrm{K}^0(\Delta t)\right] . \quad (5)$$

The measurement of any deviation from the prediction $R_{i,\mathrm{s}}(\Delta t) = 1$ imposed by the symmetry invariance (with $\mathrm{s} = \mathrm{T},\ \mathrm{CP}$ or CPT and $i = 1, 4$) is a direct and genuine signal of the corresponding symmetry violation. It is worth noting that for $\Delta t = 0$:

$$R_{1,\mathrm{s}}(0) = R_{2,\mathrm{s}}(0) = R_{3,\mathrm{s}}(0) = R_{4,\mathrm{s}}(0) = 1 , \quad (6)$$

i.e. the T, CP, CPT violating effects are built in the time evolution of the system, and are absent at $\Delta t = 0$, within our approximations. For $\Delta t \gg \tau_S$ all ratios, including the symmetry violating effects, reach an asymptotic regime (i.e. constant in Δt).

At a ϕ-factory one can define two observable ratios as a function of the difference Δt of the two kaon decay times for each symmetry test [10,11,22]:

$$R^{\mathrm{exp}}_{2,\mathrm{T}}(\Delta t) \equiv \frac{I(\pi^+e^-\overline{\nu}, 3\pi^0; \Delta t)}{I(\pi^+\pi^-, \pi^-e^+\nu; \Delta t)};$$
$$R^{\mathrm{exp}}_{4,\mathrm{T}}(\Delta t) \equiv \frac{I(\pi^-e^+\nu, 3\pi^0; \Delta t)}{I(\pi^+\pi^-, \pi^+e^-\overline{\nu}; \Delta t)} \quad (7)$$
$$R^{\mathrm{exp}}_{2,\mathrm{CP}}(\Delta t) \equiv \frac{I(\pi^+e^-\overline{\nu}, 3\pi^0; \Delta t)}{I(\pi^-e^+\nu, 3\pi^0; \Delta t)};$$
$$R^{\mathrm{exp}}_{4,\mathrm{CP}}(\Delta t) \equiv \frac{I(\pi^+\pi^-, \pi^-e^+\nu; \Delta t)}{I(\pi^+\pi^-, \pi^+e^-\overline{\nu}; \Delta t)} \quad (8)$$
$$R^{\mathrm{exp}}_{2,\mathrm{CPT}}(\Delta t) \equiv \frac{I(\pi^+e^-\overline{\nu}, 3\pi^0; \Delta t)}{I(\pi^+\pi^-, \pi^+e^-\overline{\nu}; \Delta t)};$$
$$R^{\mathrm{exp}}_{4,\mathrm{CPT}}(\Delta t) \equiv \frac{I(\pi^-e^+\nu, 3\pi^0; \Delta t)}{I(\pi^+\pi^-, \pi^-e^+\nu; \Delta t)} , \quad (9)$$

where $I(f_1, f_2; \Delta t)$ is the double decay rate into final states f_1 and f_2 as a function of $\Delta t = t_2 - t_1$ [23], with f_1 occurring before f_2 decay for $\Delta t > 0$, and vice versa for $\Delta t < 0$.

These ratios are related to the $R_{i,\mathrm{s}}(\Delta t)$ ratios defined in Eqs. (3), (4), (5) as follows, for $\Delta t \geq 0$ [10,11]:

$$R^{\mathrm{exp}}_{2,\mathrm{T}}(\Delta t) = R_{2,\mathrm{T}}(\Delta t) \times D$$
$$R^{\mathrm{exp}}_{4,\mathrm{T}}(\Delta t) = R_{4,\mathrm{T}}(\Delta t) \times D$$
$$R^{\mathrm{exp}}_{2,\mathrm{CP}}(\Delta t) = R_{2,\mathrm{CP}}(\Delta t)$$
$$R^{\mathrm{exp}}_{4,\mathrm{CP}}(\Delta t) = R_{4,\mathrm{CP}}(\Delta t)$$
$$R^{\mathrm{exp}}_{2,\mathrm{CPT}}(\Delta t) = R_{2,\mathrm{CPT}}(\Delta t) \times D$$
$$R^{\mathrm{exp}}_{4,\mathrm{CPT}}(\Delta t) = R_{4,\mathrm{CPT}}(\Delta t) \times D, \quad (10)$$

whereas for $\Delta t < 0$ one has:

$$R^{\mathrm{exp}}_{2,\mathrm{T}}(\Delta t) = R_{1,\mathrm{T}}(|\Delta t|) \times D$$
$$R^{\mathrm{exp}}_{4,\mathrm{T}}(\Delta t) = R_{3,\mathrm{T}}(|\Delta t|) \times D$$
$$R^{\mathrm{exp}}_{2,\mathrm{CP}}(\Delta t) = R_{1,\mathrm{CP}}(|\Delta t|)$$
$$R^{\mathrm{exp}}_{4,\mathrm{CP}}(\Delta t) = R_{3,\mathrm{CP}}(|\Delta t|)$$
$$R^{\mathrm{exp}}_{2,\mathrm{CPT}}(\Delta t) = R_{1,\mathrm{CPT}}(|\Delta t|) \times D$$
$$R^{\mathrm{exp}}_{4,\mathrm{CPT}}(\Delta t) = R_{3,\mathrm{CPT}}(|\Delta t|) \times D, \quad (11)$$

with D a constant factor given by [10,11,22]:

$$D = \frac{\left|\langle 3\pi^0|\mathcal{T}|\mathrm{K}_-\rangle\right|^2}{\left|\langle \pi^+\pi^-|\mathcal{T}|\mathrm{K}_+\rangle\right|^2} = \frac{\mathrm{BR}\left(\mathrm{K_L} \to 3\pi^0\right)}{\mathrm{BR}\left(\mathrm{K_S} \to \pi^+\pi^-\right)} \frac{\Gamma_L}{\Gamma_S} . \quad (12)$$

The last right hand side equality holds with a high degree of accuracy, at least $\mathcal{O}(10^{-7})$. The value of D can be therefore directly evaluated from branching ratios and lifetimes of $\mathrm{K_{S,L}}$ states. They were all directly measured by the KLOE experiment with the highest precision [24–28], and we consistently use them for the evaluation of $D = (0.5076 \pm 0.0059) \times 10^{-3}$.

For the processes under study for large differences of the two kaon decay times (asymptotic regime), it can be shown that the early and the late decaying kaon states correspond in practice to $\mathrm{K_S}$ and $\mathrm{K_L}$ states [20], respectively.[2] Intuitively, under this condition, the $\mathrm{K}_+ \to \mathrm{K}^0/\overline{\mathrm{K}}^0$ transitions are highly suppressed requiring a $\mathrm{K_S} \to 3\pi^0$ as an early decay, with a branching fraction of $\mathcal{O}(10^{-9})$. Also $\mathrm{K}^0/\overline{\mathrm{K}}^0 \to \mathrm{K}_+$ transitions are largely suppressed requiring a $\mathrm{K_S}$ semileptonic decay as the early decay, and a $\mathrm{K_L}$ CP-violating decay into two pions as the late decay, with an overall suppression factor of $\mathcal{O}(10^{-6})$. All these transitions involving a K_+ state correspond to the observable ratios with $\Delta t < 0$ (11). Transitions involving a K_- state are less suppressed having more favourable branching fractions, and correspond to the observable ratios with $\Delta t > 0$ (10).

This is more quantitatively studied with a Monte Carlo simulation, confirming that in the case of the KLOE and KLOE-2 experiments with an integrated luminosity of $\mathcal{O}(10\ \mathrm{fb}^{-1})$ the statistically most populated region for our observable ratios (7)-(9) is the $\Delta t > 0$ region and in particular with $\Delta t \gg \tau_S$ (the asymptotic region), while the region for $\Delta t < 0$ has few or no events [10].

Therefore we define eight observables (six ratios and two double ratios) that are experimentally accessible at KLOE with $\Delta t > 0$ in the asymptotic regime, i.e. constants in Δt (as can be experimentally verified)[3]:

$$R_{2,\mathrm{T}} \equiv \frac{R^{\mathrm{exp}}_{2,\mathrm{T}}(\Delta t \gg \tau_S)}{D} = 1 - 4\Re\epsilon + \left(4\Re x_+ + 4\Re y\right) , \quad (13)$$
$$R_{4,\mathrm{T}} \equiv \frac{R^{\mathrm{exp}}_{4,\mathrm{T}}(\Delta t \gg \tau_S)}{D} = 1 + 4\Re\epsilon + \left(4\Re x_+ - 4\Re y\right) , \quad (14)$$
$$R_{2,\mathrm{CP}} \equiv R^{\mathrm{exp}}_{2,\mathrm{CP}}(\Delta t \gg \tau_S) = 1 - 4\Re\epsilon_S + \left(4\Re y - 4\Re x_-\right) , \quad (15)$$
$$R_{4,\mathrm{CP}} \equiv R^{\mathrm{exp}}_{4,\mathrm{CP}}(\Delta t \gg \tau_S) = 1 + 4\Re\epsilon_L - \left(4\Re y + 4\Re x_-\right) , \quad (16)$$
$$R_{2,\mathrm{CPT}} \equiv \frac{R^{\mathrm{exp}}_{2,\mathrm{CPT}}(\Delta t \gg \tau_S)}{D} = 1 - 4\Re\delta + \left(4\Re x_+ - 4\Re x_-\right) , \quad (17)$$
$$R_{4,\mathrm{CPT}} \equiv \frac{R^{\mathrm{exp}}_{4,\mathrm{CPT}}(\Delta t \gg \tau_S)}{D} = 1 + 4\Re\delta + \left(4\Re x_+ + 4\Re x_-\right) , \quad (18)$$
$$DR_{\mathrm{T,CP}} \equiv \frac{R_{2,\mathrm{T}}}{R_{4,\mathrm{T}}} \equiv \frac{R_{2,\mathrm{CP}}}{R_{4,\mathrm{CP}}} = 1 - 8\Re\epsilon + \left(8\Re y\right) , \quad (19)$$
$$DR_{\mathrm{CPT}} \equiv \frac{R_{2,\mathrm{CPT}}}{R_{4,\mathrm{CPT}}} = 1 - 8\Re\delta - \left(8\Re x_-\right) , \quad (20)$$

where ϵ and δ are the usual T and CPT violation parameters in the neutral kaon mixing, respectively, and $\epsilon_{S,L} = \epsilon \pm \delta$ the CP impurities in the physical states $\mathrm{K_S}$ and $\mathrm{K_L}$; the small parameter y describes a possible CPT violation in the $\Delta S = \Delta Q$ semileptonic decay amplitudes, while x_+ and x_- describe $\Delta S \neq \Delta Q$ semileptonic decay amplitudes with CPT invariance and CPT violation,

[2] The states filtered by the decays are in general different from the decaying states, i.e. the states soon before the decays; moreover due to the entanglement each decaying state is undefined until the measurement of its entangled partner [20].

[3] See Ref. [29] for more general formulae valid for $\Delta t \geq 0$.

respectively. Double ratios defined in Eq. (19) and (20) are independent from the D factor.

The right hand side in Eqs. (13)-(20) are therefore assuming the presence of symmetry violations only in the effective Hamiltonian of the Weisskopf–Wigner approach [30] and no other possible symmetry violation effect. The terms in the brackets show the small possible spurious effects (to first order in small parameters) due to the release of the assumptions of the validity of the $\Delta S = \Delta Q$ rule and of negligible CPT violation in semileptonic decays. Therefore for each of the eight observables the terms in brackets precisely specify under which assumptions the corresponding symmetry test holds.

Attention must also be paid to the presence of direct CP and CPT violation contributions in the $\pi\pi$ and $3\pi^0$ decay amplitudes that could mimic T or CPT violation effects. However they turn out to be fully negligible for all observables (13)-(20) in the asymptotic region $\Delta t \gg \tau_S$ (a detailed description can be found in Refs. [10,11,29]). The CPT test with the double ratio $DR_{\rm CPT}$ is also not affected in the same region by possible violation of the $\Delta S = \Delta Q$ rule, because x_- signals also CPT violation. Therefore the double ratio (20) constitutes one of the most robust observables of our CPT test. It is independent of D, and in the limit $\Delta t \gg \tau_S$ it exhibits a pure and genuine CPT violating effect, even without the assumptions of the validity of the $\Delta S = \Delta Q$ rule and with negligible contaminations from direct CP violation.

3. The KLOE detector

The KLOE detector is located at the DAΦNE ϕ-factory [31], an e^+e^- collider operating at center-of-mass energy of $m_\phi \approx 1.020$ GeV. Collisions predominantly produce ϕ mesons nearly at rest, which decay into an entangled $K^0\overline{K}^0$ pair in 34% of cases.

The main components of the detector are a large cylindrical drift chamber (DC) and an electromagnetic calorimeter (EMC), immersed in the axial magnetic field of 0.52 T produced by a superconducting coil. The DC [32] uses a low-Z gas mixture of isobutane (10%) and helium (90%) assuring transparency to low-energy photons. The inner wall of the chamber is made of light carbon fibre composite and thin (0.1 mm) aluminum foil to minimise $K_L \to K_S$ regeneration. Vertex reconstruction resolution of the DC is about 3 mm while track momentum is reconstructed with $\sigma(p_T)/p_T \approx 0.4\%$. The large outer radius of the chamber (2 m) allows for recording about 40% of all decays of K_L produced in KLOE.

The EMC [33] consists of a barrel surrounding the DC and two endcaps, together covering 98% of the solid angle. It contains a total of 2440 cells of 4.4×4.4 cm^2 cross section, built of lead foils alternated with scintillating fibres of 1 mm diameter. Each cell is read out by photomultipliers at both ends. Energy deposits along the cells are localised using time difference between photomultiplier signals. Deposits in adjacent cells are grouped into clusters for which energy and time resolutions are $\sigma(E)/E = 0.057/\sqrt{E(\text{GeV})}$ and $\sigma(t) = 54\,\text{ps}/\sqrt{E(\text{GeV})} \oplus 100\,\text{ps}$ and position is resolved with $\sigma_\parallel = 1.4\ \text{cm}/\sqrt{E\ (\text{GeV})}$ along the fibres and $\sigma_\perp = 1.3$ cm in the orthogonal direction. The acceptance of the EMC is complemented with additional tile calorimeters covering the two final focusing quadrupole magnets of the beam line [34].

The detector operates with two different triggers [35]; the calorimeter trigger which requires at least two clusters with $E > 50$ MeV in the barrel or $E > 150$ MeV in the endcaps, and the DC trigger based on multiplicity and topology of hits in the DC. Either of the two triggers is sufficient to start the acquisition of an event. Subsequently, recorded events are subject to an on-line machine background filter based on calorimeter information only [36]. Finally, stored events are classified into physics categories based on a preliminary analysis of their topology.

4. Data analysis

The analysis was performed on a dataset collected in the years 2004–2005 with an integrated luminosity of 1.7 fb^{-1} corresponding to about 1.7×10^9 produced K_SK_L pairs and on a sample of Monte Carlo (MC) simulated events of the same size. In this period the instantaneous luminosity reached $1.5\times10^{32}\text{cm}^{-2}\text{s}^{-1}$, while trigger rates were at the level of 5 kHz.

As we are interested to select time ordered pairs of kaon decays, in the following we introduce the notation K_1 for the early decaying kaon state to final state f_1 at time t_1, and K_2 for the late decaying kaon state to final state f_2 at time t_2. Even though in the asymptotic region, $\Delta t \gg \tau_S$, K_1 and K_2 correspond in practice to K_S and K_L states [20], respectively, for sake of clarity we keep the more general $K_{1,2}$ notation, avoiding at this stage any specific identification of the decaying states.

4.1. Selection of $K_1K_2 \to (\pi^\pm e^\mp \nu)(3\pi^0)$ events

$K^0 \to K_-$ and $\overline{K}^0 \to K_-$ transitions are experimentally identified by events with an early semileptonic decay of a neutral kaon and a later decay of its entangled partner into $3\pi^0$. Presence of a vertex formed by two tracks of opposite charge is required in a cylindrical volume limited by $\rho = \sqrt{x^2+y^2} < 3$ cm and $|z| < 4.5$ cm around the average e^+e^- interaction point (IP) where z is the longitudinal and x, y are the transverse coordinates.

The $K_1 \to \pi^+\pi^-$ decays constitute the predominant source of background for semileptonic events. In order to remove this background we assume that both charged particles are pions, calculate the invariant mass and reject events with $m_{\pi\pi} > 490$ MeV.

After the reduction of data volume with the preselection based on $K_1 \to \pi^\pm e^\mp \nu$ vertex identification, the $K_2 \to 3\pi^0 \to 6\gamma$ decay is reconstructed. Presence of at least six clusters in the calorimeter not associated to tracks in the DC each with $E > 20$ MeV is required. The location and time of the K_2 decay are reconstructed using trilateration [37]. While four recorded photons are sufficient for vertex reconstruction, only events with exclusive detection of all six photons are used in the analysis to minimise background from $K_1 \to 2\pi^0$ which results in a four-photon final state. Moreover, the requirement of six recorded photons provides additional information used for enhancing the resolution of vertex reconstruction.

If an event contains seven or more candidate clusters, all combinatorial choices of six are considered and sets of six photons detected are accepted if the total energy of six clusters is between 350 MeV and 700 MeV and the calculated 6γ invariant mass is greater than 350 MeV. Moreover, for each 6-cluster set the decay vertex is reconstructed independently for each choice of 4γ subsets and results are compared providing a test sensitive to presence of photons not originating from the K_2 decay point. In case of more than one set of six clusters surviving the cuts, the spread of vertices reconstructed from each of its 4γ subsets is calculated and the set of six clusters providing the least spread is selected. The accuracy of the path length and decay time (in terms of proper time) of K_2 flight is 1.3 cm and 1.6 τ_S, respectively, for the vertices up to 160 cm distance from the IP.

At this stage, 98% of selected K_2 decays are $3\pi^0$ but the early decays are still dominated by $\pi^+\pi^-$, therefore a time of flight analysis is applied to the tracks of the early decay. The two tracks are extrapolated from the DC to the EMC and differences $\delta t(X)$ between their recorded time of flight TOF and time expected from the track length L assuming particle mass m_X are calculated as follows:

$$\delta t(X) = TOF - \frac{L}{c\beta(X)}, \quad \beta(X) = \frac{p}{\sqrt{p^2+m_X^2}}. \tag{21}$$

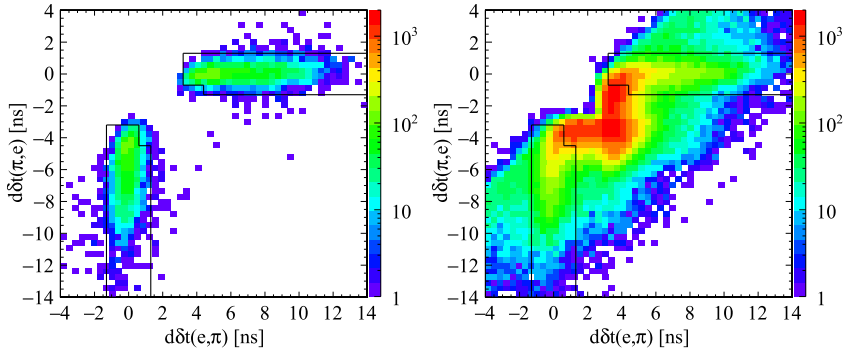

Fig. 1. Distribution of $d\delta t(\pi, e)$ vs $d\delta t(e, \pi)$ for $K_1K_2 \to (\pi^{\pm}e^{\mp}\nu)(3\pi^0)$ MC-simulated events (left) and all data events (right). Solid lines denote accepted regions, each corresponding to one possible assignment of pion and electron mass hypotheses to the two DC tracks in an event.

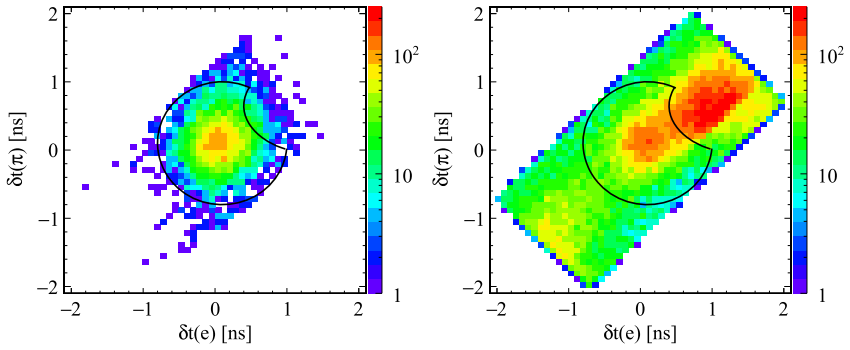

Fig. 2. Distribution of $\delta t(\pi)$ vs $\delta t(e)$ after particle identification for MC-simulated $K_1K_2 \to (\pi^{\pm}e^{\mp}\nu)(3\pi^0)$ events (left) and all data events (right). Events inside the region marked with black solid line are accepted.

Comparison of the differences of δt between the two tracks, $d\delta t(X, Y) = \delta t_{trk1}(X) - \delta t_{trk2}(Y)$, in case of two possible assignments of particle masses allows for efficient rejection of $\pi^+\pi^-$ background as well as for identification of pion and electron tracks. Events are accepted if they satisfy the following condition, $|d\delta t(\pi, \pi)| \in (1.5,\ 10)$ ns, and the selection in the $d\delta t(\pi, e)$ vs $d\delta t(e, \pi)$ plane, as shown in Fig. 1.

After the pion and electron tracks are identified, a second cut is applied in the $\delta t(\pi)$ *vs* $\delta t(e)$ plane as shown in Fig. 2 to further discriminate the remaining $\pi^+\pi^-$ events. After these cuts, background remains (amounting to about 12% of the event sample) constituted by the $K_1 \to \pi^0\pi^0$ and $K_2 \to \pi e\nu$ processes where the K_1 decay along with additional clusters had been misidentified as a $K_2 \to 3\pi^0$ decay. This background is suppressed by removing events containing more than one cluster for which $R/(cT_{clu}) > 0.9$ where R is the distance between the IP and the cluster (corresponding to photons emitted close to the IP).

The remaining background (in the order of decreasing contribution) is composed of:

- $K_1 \to \pi^+\pi^-$ with imperfect track reconstruction,
- $K_1 \to \pi^+\pi^- \to \pi\mu\nu$ decay chain where one of the charged pions decays into a muon and a neutrino before entering the DC,
- radiative $K_1 \to \pi^+\pi^-\gamma$ decays dominated by inner bremsstrahlung [38,39].

As all these events are characterised by a pion or muon track misidentified as e^+/e^-, two particle binary classifiers based on Artificial Neural Networks (ANNs) (using Multilayer Perceptron from the TMVA package [40]) and acting on an ensemble constituted by a track and its associated cluster are prepared for e/π and μ/π discrimination in subsequent steps. Classification is based on the different structure of the energy deposited in the EMC cells by electrons, pions, and muons, in combination with the information of the particle momentum from the associated DC track. The ANNs are trained using data control samples of $K_2 \to \pi^{\pm}e^{\mp}\nu$ and $K_2 \to \pi^{\pm}\mu^{\mp}\nu$ decays tagged by $K_1 \to \pi^+\pi^-$ identified with a 98% purity according to MC simulations.

After the e/π and e/μ particle discrimination for lepton track candidates, the signal to background ratio amounts to 22.5 with residual background dominated by $K_1 \to \pi^+\pi^-$ (55%), $K_1 \to \pi^+\pi^-\gamma$ (19%) and events with K_2 decays to other than $3\pi^0$ (12%). The distribution of the residual background as a function of Δt is modelled with an exponential function presented in Fig. 3. Parameters of the exponential models are obtained with a fit to MC residual background separately for event samples with an electron and positron with χ^2/NDF of 2.1 and 0.99 respectively. These models are used to subtract the expected background contamination from the data distributions shown in black points in Fig. 3.

4.2. *Selection of* $K_1K_2 \to (\pi^+\pi^-)(\pi^{\pm}e^{\mp}\nu)$ *events*

As $K_- \to K^0$ and $K_- \to \overline{K}^0$ transitions are characterised by an early kaon decay into two pions (the $\pi^+\pi^-$ final state is chosen in this analysis) followed by a later semileptonic decay, the event selection requires the presence of a DC vertex associated to 2 opposite curvature tracks within a cylindrical volume of $\rho < 15$ cm and $|z| < 10$ cm around the IP and with $|m_{\pi\pi} - m_{K^0}| < 10$ MeV.

To find the semileptonic decay vertex, all vertices formed by two opposite curvature tracks in the DC are considered, excluding the previously identified $K_1 \to \pi^+\pi^-$ vertex and its related

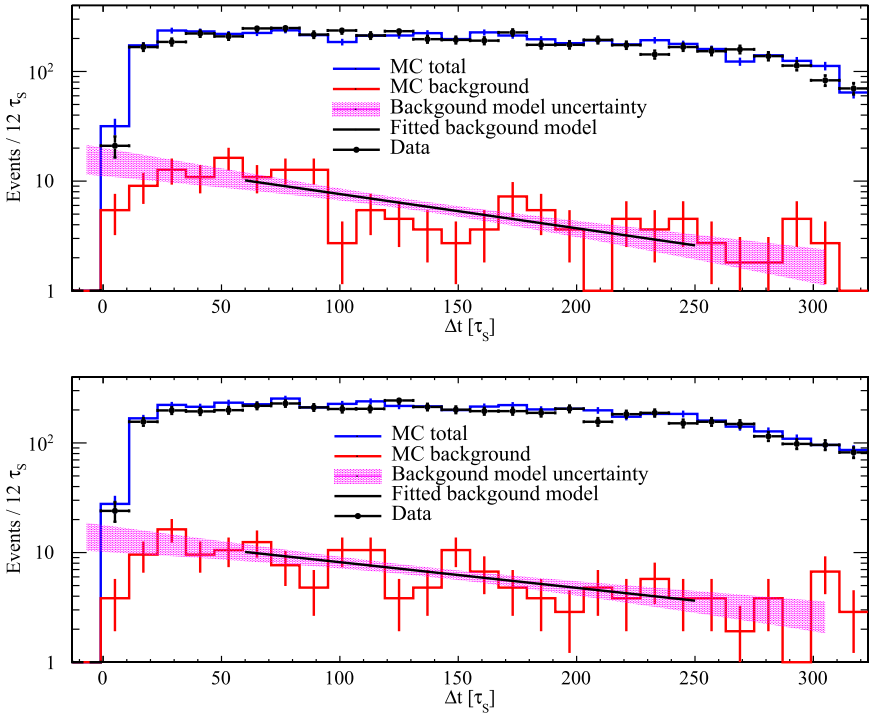

Fig. 3. $K_1K_2 \to (\pi^\pm e^\mp \nu)(3\pi^0)$ sample: exponential model of residual background distribution as a function of Δt for events with an electron (top) and positron (bottom) in the early kaon semileptonic decay. The modelled expected background is obtained in a fit to MC residual background and subtracted from the respective data distributions. The uncertainty of the fitted models (magenta band) is taken into account as a source of systematic uncertainty.

tracks. For each candidate semileptonic vertex the following invariant mass (which for correct e/π identification should correspond to the electron mass) is evaluated separately for each track:

$$m_\pm^2 = (E_K - E(\pi)_\mp - |\vec{p}_{miss}|)^2 - |\vec{p}_\pm|^2, \tag{22}$$

with E_K being the energy of the decaying kaon, $E(\pi)_\mp$ the energy attributed to the track of negative (positive) charge assuming the charged pion mass, $\vec{p}_\pm$ the momentum corresponding to the positive (negative) charge track, and $\vec{p}_{miss} = \vec{p}_K - \vec{p}_+ - \vec{p}_-$. In the dominant background sources ($\pi^+\pi^-\pi^0$ and semileptonic decays with a muon) both tracks are characterised by significant m^2 values whereas for genuine $\pi^\pm e^\mp \nu$ decays $m^2 \approx 0$ for one of the tracks, making the sum of m^2 for both tracks in the event sensitive to a difference between $K_2 \to \pi^\pm e^\mp \nu$ vertices and other decays as shown in Fig. 4. Vertex candidates with $m_+^2 + m_-^2 > 0.015\ (\mathrm{GeV})^2$ are rejected and only events with one remaining vertex candidate are considered in further analysis.

Further selection of semileptonic decays of K_2 as well as identification of the $e^\pm$ and $\pi^\pm$ tracks is performed with a time of flight analysis similarly as in the case of $K_1 \to \pi^\pm e^\mp \nu$, resulting in signal to background ratio of 75. The remaining background is neglected in further analysis.

4.3. Determination of efficiencies

For each of the two classes of processes, selected events are split by charge of the electron and positron from the semileptonic decay. Δt-dependent efficiencies are evaluated separately for each of the obtained four samples of events as:

$$\varepsilon_{total}(\Delta t) = \varepsilon_{TEC} \times \varepsilon_{SEL}(\Delta t), \tag{23}$$

where ε_{TEC} is the combination of Δt-independent efficiencies of trigger, machine background filter and event classification described in Section 3 and $\varepsilon_{SEL}(\Delta t)$ represents the efficiency of event selection (cuts) for a particular Δt interval.

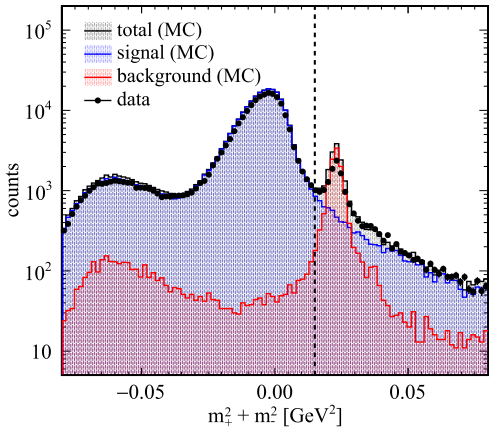

Fig. 4. Sum of invariant masses of two decay product tracks assuming their electron mass hypotheses and a semileptonic decay. Background and data distributions contain contributions from different decay vertex choices. K_2 decay vertex candidates with $m_+^2 + m_-^2 > 0.015\ (\mathrm{GeV})^2$ (i.e. right of the dashed vertical line) are rejected.

For evaluation of the trigger efficiency, rates of events with either one – EMC or DC based – or both triggers for events passing the entire event selection, are used to obtain the total probability of at least one of the triggers fulfilled on a signal event. Efficiency of the machine background filter is estimated by counting events passing the signal selection criteria among 10% of all events acquired independently of the filter decision. Similarly, a subsample of 5% of all events stored independently of their classification is used to evaluate the probability of misclassification of a signal event and thus the classification efficiency. Table 1 summarises the ε_{TEC} efficiencies combining these three factors for each class of signal events.

Table 1
Combined efficiencies of trigger, machine background filter and event classification for the four event samples.

event sample	ε_{TEC} [%]
$K_1K_2 \to (\pi^+e^-\nu)\,(3\pi^0)$	99.487 ± 0.071
$K_1K_2 \to (\pi^-e^+\nu)\,(3\pi^0)$	99.453 ± 0.074
$K_1K_2 \to (\pi^+\pi^-)\,(\pi^+e^-\nu)$	99.597 ± 0.007
$K_1K_2 \to (\pi^+\pi^-)\,(\pi^-e^+\nu)$	99.589 ± 0.010

Table 2
Numbers of events identified for each of the four event classes. The background contamination is 4% for the first event sample, and 1% for the second one.

event sample	events
$K_1K_2 \to (\pi^+e^-\nu)\,(3\pi^0)$	4750
$K_1K_2 \to (\pi^-e^+\nu)\,(3\pi^0)$	4652
$K_1K_2 \to (\pi^+\pi^-)\,(\pi^+e^-\nu)$	15924863
$K_1K_2 \to (\pi^+\pi^-)\,(\pi^-e^+\nu)$	15708190

Event selection efficiencies are estimated using Monte Carlo simulations of the respective event classes. Due to the relatively low branching ratio of the semileptonic $K_1 \to \pi e\nu$ decay, the efficiencies for identifying $K_1K_2 \to \pi e\nu\, 3\pi^0$ events are affected by large fluctuations caused by low statistics of MC events per bin. Therefore, a smoothing procedure is applied to the efficiency Δt distributions. In case of semileptonic decays, MC-based efficiencies $\varepsilon_{SEL}(\Delta t)$ are corrected using an independent data control sample of $K_1K_2 \to (\pi^0\pi^0)(\pi^\pm e^\mp\nu)$ events. The selection efficiency for $K_2 \to 3\pi^0$ decays is estimated with MC and corrected with a $K_1K_2 \to (\pi^+\pi^-)(3\pi^0)$ data control sample. The $K_2 \to \pi^\pm e^\mp\nu$ decays from the control sample are selected in the same manner as signal events, but from the sample selected with $\pi^0\pi^0$ decays. These neutral K_1 decays are selected based on the sum of the energies of four clusters and their timing as well as the reconstructed invariant mass of the kaon. Selection of $K_2 \to 3\pi^0$ decays from the second control sample is performed in an analogous way as for signal events, but the sample selected with $\pi^+\pi^-$ decays. These K_1 decays are identified within a fiducial volume around the IP selecting a single vertex constructed with exactly two tracks with opposite charge and a total momentum and an invariant mass for these two tracks inside the kinematic cut.

Finally, the relative MC-based efficiencies entering the observable ratios in Eqs. (7)-(9) for the selection of $K_1 \to \pi^+e^-\overline{\nu}$, $K_1 \to \pi^-e^+\nu$, and $K_1 \to \pi^+\pi^-$ decays, are modified with a constant correction factor, using independent control samples containing the relevant K_1 decays tagged by a K_2 interaction in the KLOE calorimeter.

5. Ratios of double kaon decay rates

After the event selection, the counts of events identified for each class are presented in Table 2. The differences in the number of events among the different classes are due to the differences of branching ratios for given channels. Fig. 5 shows a summary of the corresponding data Δt distributions entering the probability ratios along with their respective $\varepsilon_{SEL}(\Delta t)$ event selection efficiencies in the range $0 < \Delta t < 320\,\tau_S$, with a bin width of $12\,\tau_S$.

The T and CPT-violation sensitive single ratios defined in Eqs. (7) and (9) are shown in Figs. 6 and 7. Each point of the single ratio graphs is defined through the counts of the respective double kaon decays N_i and N'_i in the i-th interval of Δt and their corresponding event identification efficiencies ε_i and ε'_i as:

$$R_i \equiv R(\Delta t_i) = \frac{N_i}{N'_i}\frac{\varepsilon'_i}{\varepsilon_i}\frac{1}{D}, \tag{24}$$

where D is the factor defined in Eq. (12).

Due to the limited statistics of the process entering the numerator of the ratios, a value of the single ratios is evaluated in the range of high and relatively stable efficiency of $\Delta t \in (47, 275)\tau_S$ using a maximum likelihood fit for the constant ratio R_S:

$$\mathcal{L}(R_S) = \prod_{i \text{ in fit limits}} p\left(N_i,\ R_S N'_i D\frac{\varepsilon_i}{\varepsilon'_i}\right), \tag{25}$$

where $p(n, \lambda)$ is the Poissonian probability of observing n counts with the distribution mean of λ.

Counts of the $K_1K_2 \to (\pi^+\pi^-)(\pi^\pm e^\mp\nu)$ events with a positron and an electron are also used to construct transition rate ratios sensitive to CP-violation (Eq. (8)) shown in Fig. 8. Finally, double ratios sensitive to T and CP violation (Eq. (19)) and CPT violation (Eq. (20)) are constructed and their asymptotic levels are estimated as presented in Fig. 9.

6. Systematic uncertainties

The stability of the results is checked by varying the event selection cut values by $\pm 5\sigma$ in steps of 1σ where σ denotes the resolution on the variable subject to the cut, repeating the analysis for each cut value and observing the impact of variation on each of the eight observables of the tests. For evaluation of the corresponding systematic uncertainties absolute deviations of each of the observables for $\pm 1\sigma$ cut variation are averaged.

The uncertainty due to the model of subtracted background is estimated by varying the two model parameters within their errors. Effects from $\pm 1\sigma$ variations of each parameter of the model are added in quadrature.

Event selection efficiencies based on MC simulations with limited statistics are subject to a smoothing procedure. The corresponding systematic uncertainty is quantified by comparing analysis results with and without efficiency smoothing.

The choice of Δt bin width for the final ratio distributions and the fit limits account for another source of systematic uncertainty. Stability of the fit results is tested for bin widths ranging from $3\ \tau_S$ to $24\ \tau_S$ and an average of the observables' deviations obtained with the extreme bin widths from the result with $12\ \tau_S$ is used as an estimate of the systematic effect. The fitting range is varied by $\pm 24\ \tau_S$ in steps of $\pm 6\ \tau_S$ as a shift as well as total width. Changes of the fitted ratio levels for variations of one bin width ($\pm 12\ \tau_S$) are averaged and added in quadrature.

Table 3 summarises all identified systematic effects on each of the eight observables of the tests. All contributions are added in quadrature to obtain the total systematic uncertainties indicated in bold. In case of single ratios, the results are additionally affected by the total error on the D factor (quoted separately due to containing both statistical and systematic contributions) obtained from previous KLOE measurements.

7. Results and conclusions

We presented the first direct tests of T, CP, CPT symmetries in transitions of neutral kaons, obtained analysing 1.7 fb^{-1} of data collected by the KLOE experiment at DAΦNE. The T and CPT tests involving time-reversal implement the necessary exchange of *in* and *out* states, as required for a genuine test, exploiting the entanglement of the $K^0\overline{K}^0$ pairs. The decay intensities of the processes $\phi \to K_SK_L \to \pi^+\pi^-\pi e\nu$ and $\phi \to K_SK_L \to \pi e\nu\, 3\pi^0$ as a function of Δt are measured in the asymptotic region $\Delta t \gg \tau_S$, statistically the most significant. We get results for all eight observables defined in Eqs. (13)–(20):

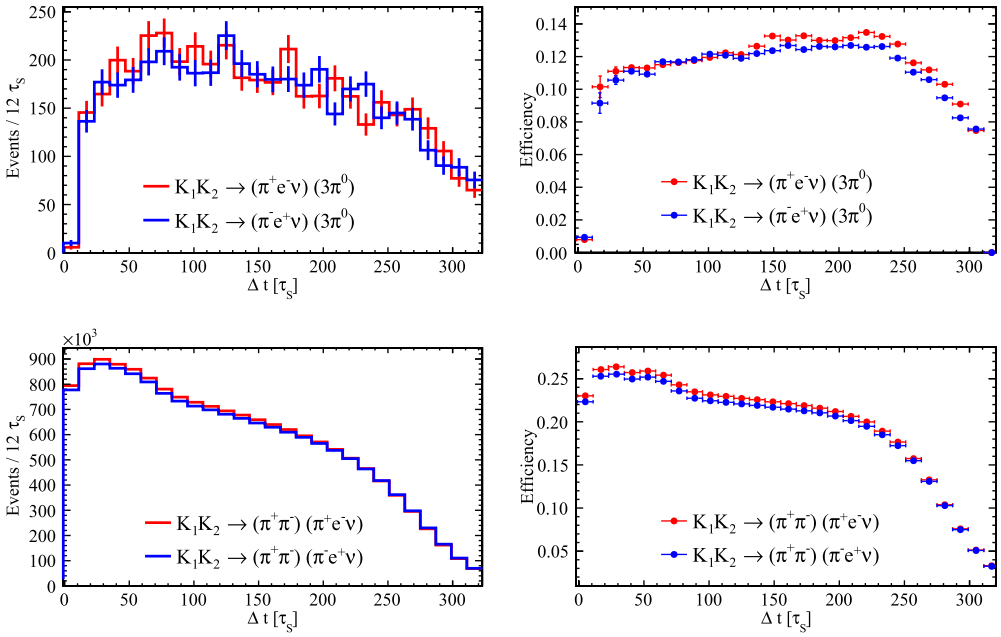

Fig. 5. Left column: Rates of double kaon decays as a function of Δt for the two studied classes of processes and two lepton charge subsamples. Right column: corresponding $\varepsilon_{SEL}(\Delta t)$ efficiencies.

Table 3
Systematic uncertainties on all of the symmetry test observables. In case of $R_{2,\mathrm{CP}}$ and $R_{4,\mathrm{CP}}$, each ratio is obtained using only one class of events and thus not affected by effects of selection of the other class. The uncertainty of the D factor comprises both statistical and systematic errors.

Effect	$R_{2,\mathrm{T}}$ $\times 10^{-3}$	$R_{4,\mathrm{T}}$ $\times 10^{-3}$	$R_{2,\mathrm{CPT}}$ $\times 10^{-3}$	$R_{4,\mathrm{CPT}}$ $\times 10^{-3}$	$DR_{\mathrm{T,CP}}$ $\times 10^{-3}$	DR_{CPT} $\times 10^{-3}$	$R_{2,\mathrm{CP}}$ $\times 10^{-3}$	$R_{4,\mathrm{CP}}$ $\times 10^{-3}$
Background model	2.74	4.62	2.79	4.43	4.43	4.41	4.37	–
Efficiency smoothing	2.46	5.31	2.43	5.26	6.70	6.83	6.76	0.17
Δt bin width	8.00	5.00	7.50	5.50	9.00	9.00	8.90	0.03
Fit range	7.33	8.88	7.32	8.84	7.95	7.60	7.78	0.41
Effects of cuts in the $K_1K_2 \to (\pi e\nu)(3\pi^0)$ selection								
K_1 vertex location cuts	0.57	2.31	0.58	2.27	2.36	2.41	2.39	–
$M(\pi,\pi)$ cut	2.48	1.34	2.52	1.31	1.56	1.63	1.60	–
TOF cuts	6.08	5.32	6.19	5.23	6.40	6.58	6.49	–
$e/\pi/\mu$ classification	4.78	4.40	4.85	4.33	9.33	9.59	9.46	–
Effects of cuts in the $K_1K_2 \to (\pi^+\pi^-)(\pi e\nu)$ selection								
K_1 vertex location cuts	0.007	0.004	0.004	0.007	0.004	0.004	–	0.005
$M(\pi,\pi)$ and $\lvert\vec{p}\rvert$ cuts	2.14	1.68	1.67	2.17	0.70	0.72	–	0.74
$m_+^2 + m_-^2$ cut	1.48	1.32	1.31	1.49	0.20	0.21	–	0.21
TOF cuts	2.14	1.68	1.67	2.17	0.70	0.72	–	0.74
Total systematic uncertainty	**14**	**15**	**14**	**15**	**19**	**19**	**19**	**0.89**
D factor total uncertainty	12	12	12	12	–	–	–	–

$$R_{2,\mathrm{T}} = 0.991 \pm 0.017_{stat} \pm 0.014_{syst} \pm 0.012_D \,, \quad (26)$$

$$R_{4,\mathrm{T}} = 1.015 \pm 0.018_{stat} \pm 0.015_{syst} \pm 0.012_D \,, \quad (27)$$

$$R_{2,\mathrm{CPT}} = 1.004 \pm 0.017_{stat} \pm 0.014_{syst} \pm 0.012_D \,, \quad (28)$$

$$R_{4,\mathrm{CPT}} = 1.002 \pm 0.017_{stat} \pm 0.015_{syst} \pm 0.012_D \,, \quad (29)$$

$$R_{2,\mathrm{CP}} = 0.992 \pm 0.028_{stat} \pm 0.019_{syst} \,, \quad (30)$$

$$R_{4,\mathrm{CP}} = 1.00665 \pm 0.00093_{stat} \pm 0.00089_{syst} \,, \quad (31)$$

$$DR_{\mathrm{T,CP}} = R_{2,\mathrm{T}}/R_{4,\mathrm{T}} = 0.979 \pm 0.028_{stat} \pm 0.019_{syst} \,, \quad (32)$$

$$DR_{\mathrm{CPT}} = R_{2,\mathrm{CPT}}/R_{4,\mathrm{CPT}} = 1.005 \pm 0.029_{stat} \pm 0.019_{syst} \,. \quad (33)$$

A comparison of these results with expected values (assuming CPT invariance, the validity of the $\Delta S = \Delta Q$ rule, and T violation extrapolated from observed CP violation in the mixing [28]) is presented in Fig. 10. Each ratio measurement should be regarded as an independent symmetry test on its own. However a correlation among them is present because the same transitions are used in different tests, as can be easily deduced from Eqs. (3), (4), (5).

For the T and CPT single ratios a total relative error of 2.5% is reached, while for the double ratios (19) and (20) the total error increases to 3.5%, with the advantage of improved sensitivity to violation effects, and of independence from the D factor. The measurement of the single ratio $R_{4,\mathrm{CP}}$ benefits of highly allowed decay rates for the involved channels, reaching an error of 0.13%.

All tests with single ratios assume the validity of the $\Delta S = \Delta Q$ rule and CPT invariance in semileptonic decay, as specified in

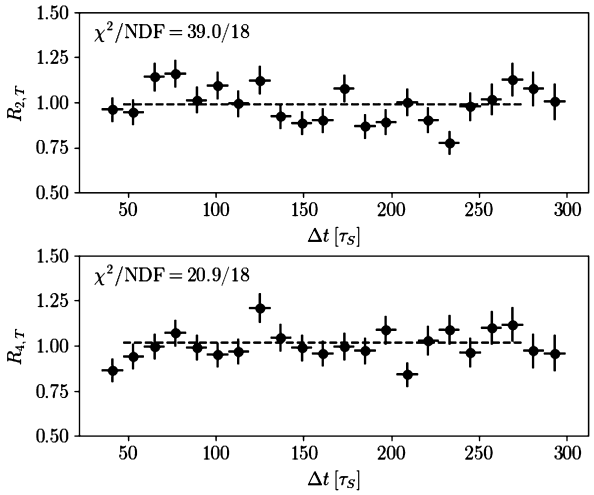

Fig. 6. T-violation sensitive ratios of double decay rates as defined in Eq. (7). Dashed lines denote the fit of the single parameter, level of the line, to the data points (see Eq. (13) and (14)). The obtained value together with statistical uncertainty is presented in Eq. (26) and (27).

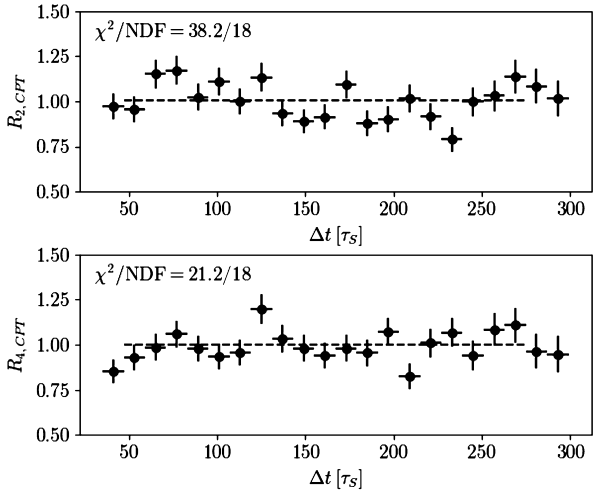

Fig. 7. CPT-violation sensitive ratios of double decay rates as defined in Eq. (9). Dashed lines denote the fit of the single parameter, level of the line, to the data points (see Eq. (17) and (18)). The obtained value together with statistical uncertainty is presented in Eq. (28) and (29).

Eqs. (13)–(20).[4] The double ratio DR_{CPT} is our best observable for testing CPT, free from approximations and model independent, while $DR_{\mathrm{T,CP}}$ assumes no direct CPT violation in semileptonic decays and is even under a CPT transformation, therefore it does not disentangle T and CP violation effects, contrary to the genuine T and CP single ratios.

The results on T and CPT observables show no evidence of symmetry violation. They constitute the first test of these symmetries performed in transitions of neutral kaons. We observe CP violation for the first time in $K_- \to K^0/\overline{K}^0$ transitions in the single ratio $R_{4,\mathrm{CP}}$ with a significance of 5.2σ, in agreement with the known CP violation in the $K^0 - \overline{K}^0$ mixing, and differently from the CPLEAR measurement involving $K^0/\overline{K}^0 \to K_+$ transitions [41].

[4] The experimental limits on the corresponding violation parameters $\Re y$, $\Re x_-$, $\Re x_+$ are of $\mathcal{O}(10^{-3})$ [28].

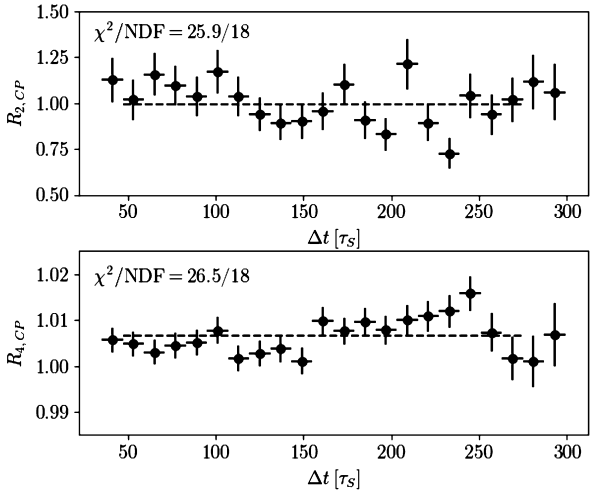

Fig. 8. CP-violation sensitive ratios of double decay rates as defined in Eq. (8). Dashed lines denote the fit of the single parameter, level of the line, to the data points (see Eq. (15) and (16)). The obtained value together with statistical uncertainty is presented in Eq. (30) and (31).

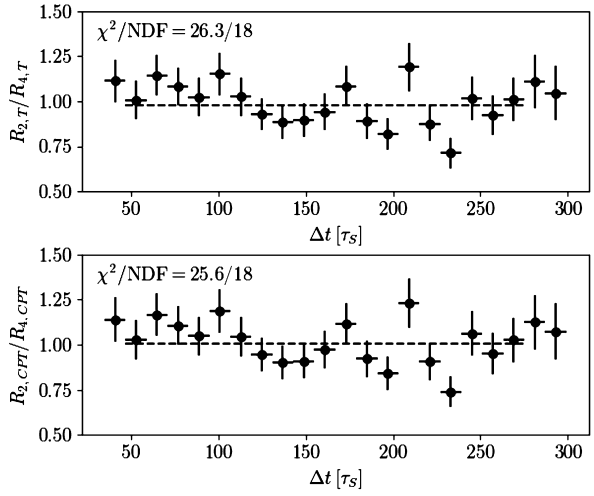

Fig. 9. Double ratios of double kaon decay rates sensitive to effects of T and CP violation (top) and CPT violation (bottom). Dashed lines denote the fit of the single parameter, level of the line, to the data points (see Eq. (19) and (20)). The obtained value together with statistical uncertainty is presented in Eq. (32) and (33).

Declaration of competing interest

The authors declare that they have no known competing financial interests or personal relationships that could have appeared to influence the work reported in this paper.

Data availability

Data will be made available on request.

Acknowledgements

We warmly thank our former KLOE colleagues for the access to the data collected during the KLOE data taking campaign. We thank the DAΦNE team for their efforts in maintaining good running conditions and their collaboration during both the KLOE run and the KLOE-2 data taking with an upgraded collision scheme [42,43]. We are very grateful to our colleague G. Capon for his enlightening comments and suggestions about the manuscript. We want to thank our technical staff: G.F. Fortugno and F. Sborzacchi for their dedication in ensuring effi-

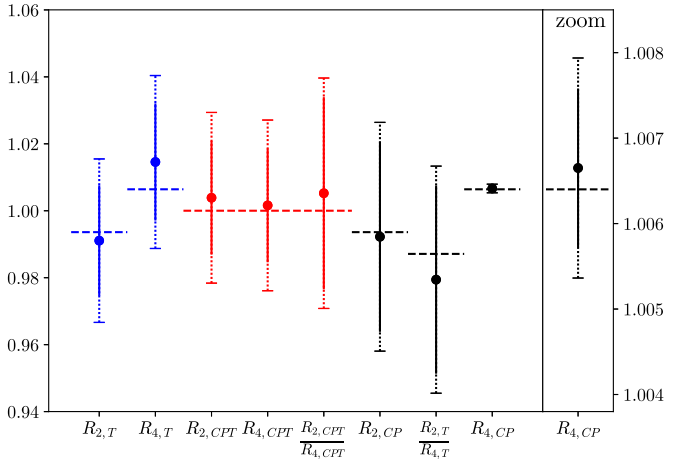

Fig. 10. Comparison of the measured symmetry-violation-sensitive single and double ratios and their expected values (horizontal dashed lines) assuming CPT invariance, the validity of the $\Delta S = \Delta Q$ rule and T violation extrapolated from observed CP violation in the mixing [28]. Solid error bars denote statistical uncertainties and dotted error bars represent total uncertainties (including error on the D factor in case of single T and CPT-violation sensitive ratios). The right-hand-side panel magnifies the region of the CP-violation-sensitive ratio $R_{4,\mathrm{CP}}$.

cient operation of the KLOE computing facilities; M. Anelli for his continuous attention to the gas system and detector safety; A. Balla, M. Gatta, G. Corradi and G. Papalino for electronics maintenance; C. Piscitelli for his help during major maintenance periods. This work was supported in part by the Polish National Science Centre through the Grants No. 2014/14/E/ST2/00262, 2016/21/N/ST2/01727, 2017/26/M/ST2/00697. A.G. acknowledges the support from the Foundation for Polish Science through grant TEAM POIR.04.04.00-00-4204/17.

References

[1] E.P. Wigner, Group Theory and its Application to the Quantum Mechanics of Atomic Spectra, Academic Press, 1959.
[2] L. Wolfenstein, The search for direct evidence for time reversal violation, Int. J. Mod. Phys. E 8 (1999) 501–511, https://doi.org/10.1142/S0218301399000343.
[3] L. Wolfenstein, Violation of time reversal invariance in K^0 decays, Phys. Rev. Lett. 83 (1999) 911–912, https://doi.org/10.1103/PhysRevLett.83.911.
[4] M.C. Banuls, J. Bernabéu CP, T and CPT versus temporal asymmetries for entangled states of the B_d-system, Phys. Lett. B 464 (1999) 117–122, https://doi.org/10.1016/S0370-2693(99)01043-6, arXiv:hep-ph/9908353.
[5] M.C. Banuls, J. Bernabéu, Studying indirect violation of CP, T and CPT in a B-factory, Nucl. Phys. B 590 (2000) 19–36, https://doi.org/10.1016/S0550-3213(00)00548-4, arXiv:hep-ph/0005323.
[6] J. Bernabéu, F. Martinez-Vidal, P. Villanueva-Perez, Time reversal violation from the entangled $B^0\overline{B}^0$ system, J. High Energy Phys. 08 (2012) 064, https://doi.org/10.1007/JHEP08(2012)064, arXiv:1203.0171.
[7] J.P. Lees, et al., Observation of time reversal violation in the B^0 meson system, Phys. Rev. Lett. 109 (2012) 211801, https://doi.org/10.1103/PhysRevLett.109.211801, arXiv:1207.5832.
[8] E. Applebaum, A. Efrati, Y. Grossman, Y. Nir, Y. Soreq, Subtleties in the *BABAR* measurement of time-reversal violation, Phys. Rev. D 89 (2014) 076011, https://doi.org/10.1103/PhysRevD.89.076011, arXiv:1312.4164.
[9] J. Bernabéu, F.J. Botella, M. Nebot, Genuine T, CP, CPT asymmetry parameters for the entangled B_d system, J. High Energy Phys. 06 (2016) 100, https://doi.org/10.1007/JHEP06(2016)100, arXiv:1605.03925.
[10] J. Bernabéu, A. Di Domenico, P. Villanueva-Perez, Direct test of time-reversal symmetry in the entangled neutral kaon system at a ϕ-factory, Nucl. Phys. B 868 (2013) 102–119, https://doi.org/10.1016/j.nuclphysb.2012.11.009, arXiv:1208.0773.
[11] J. Bernabéu, A. Di Domenico, P. Villanueva-Perez, Probing CPT in transitions with entangled neutral kaons, J. High Energy Phys. 10 (2015) 139, https://doi.org/10.1007/JHEP10(2015)139, arXiv:1509.02000.
[12] A. Angelopoulos, et al., First direct observation of time reversal noninvariance in the neutral kaon system, Phys. Lett. B 444 (1998) 43–51, https://doi.org/10.1016/S0370-2693(98)01356-2.
[13] J. Bernabéu, F. Martinez-Vidal, Colloquium: time-reversal violation with quantum-entangled B mesons, Rev. Mod. Phys. 87 (2015) 165, https://doi.org/10.1103/RevModPhys.87.165, arXiv:1410.1742.
[14] A. Angelopoulos, et al., A determination of the CPT violation parameter Re(δ) from the semileptonic decay of strangeness tagged neutral kaons, Phys. Lett. B 444 (1998) 52–60, https://doi.org/10.1016/S0370-2693(98)01357-4.
[15] G. Luders, Proof of the TCP theorem, Ann. Phys. 2 (1957) 1–15, https://doi.org/10.1016/0003-4916(57)90032-5.
[16] W. Pauli, Exclusion Principle, Lorentz Group and Reflection of Space-Time and Charge, Pergamon, London, UK, 1955, pp. 30–51.
[17] J.S. Bell, Time reversal in field theory, Proc. R. Soc. Lond. A 231 (1955) 479–495, https://doi.org/10.1098/rspa.1955.0189.
[18] R. Jost, Eine Bemerkung zum CPT-theorem, Helv. Phys. Acta 30 (1957) 409–416.
[19] D. Babusci, et al., Precision tests of quantum mechanics and $\mathcal{CPT}$ symmetry with entangled neutral kaons at KLOE, J. High Energy Phys. 04 (2022) 059, https://doi.org/10.1007/JHEP04(2022)059, arXiv:2111.04328.
[20] J. Bernabéu, A. Di Domenico, Can future observation of the living partner post-tag the past decayed state in entangled neutral K mesons?, Phys. Rev. D 105 (11) (2022) 116004, https://doi.org/10.1103/PhysRevD.105.116004, arXiv:1912.04798.
[21] C.O. Dib, B. Guberina, Almost forbidden Delta Q = - Delta S processes, Phys. Lett. B 255 (1991) 113–116, https://doi.org/10.1016/0370-2693(91)91149-P.
[22] A. Di Domenico, Testing discrete symmetries in transitions with entangled neutral kaons, Acta Phys. Pol. B 48 (2017) 1919, https://doi.org/10.5506/APhysPolB.48.1919.
[23] INFN, Handbook on Neutral Kaon Interferometry at a Φ-Factory, Frascati Physics Series, vol. 43, INFN, Frascati, Italy, 2007, http://www.lnf.infn.it/sis/frascatiseries/Volume43/volume43.pdf.
[24] F. Ambrosino, et al., Measurement of the K_L meson lifetime with the KLOE detector, Phys. Lett. B 626 (2005) 15–23, https://doi.org/10.1016/j.physletb.2005.08.022, arXiv:hep-ex/0507088.
[25] F. Ambrosino, et al., Measurements of the absolute branching ratios for the dominant K_L decays, the K_L lifetime, and V_{us} with the KLOE detector, Phys. Lett. B 632 (2006) 43–50, https://doi.org/10.1016/j.physletb.2005.10.018, arXiv:hep-ex/0508027.
[26] F. Ambrosino, et al., Precise measurement of $\Gamma(K_S \to \pi^+\pi^-(\gamma))/\Gamma(K_S \to \pi^0\pi^0)$ with the KLOE detector at DAΦNE, Eur. Phys. J. C 48 (2006) 767–780, https://doi.org/10.1140/epjc/s10052-006-0021-9, arXiv:hep-ex/0601025.
[27] F. Ambrosino, et al., Precision measurement of K_S meson lifetime with the KLOE detector, Eur. Phys. J. C 71 (2011) 1604, https://doi.org/10.1140/epjc/s10052-011-1604-7, arXiv:1011.2668.
[28] P. Zyla, et al., Review of Particle Physics, PTEP 2020 (8) (2020) 083C01, https://doi.org/10.1093/ptep/ptaa104.
[29] A. Di Domenico, Entanglement, CPT and neutral kaons, in: Proceedings of the 9th Meeting on CPT and Lorentz Symmetry, Bloomington, Indiana, USA, May 17-26, 2022, 2022, arXiv:2208.06789.
[30] V. Weisskopf, E. Wigner, Over the natural line width in radiation of the harmonius oscillator, Z. Phys. 65 (1930) 18.
[31] A. Gallo, et al., DAFNE status report, Conf. Proc. C 060626 (2006) 604–606.
[32] M. Adinolfi, F. Ambrosino, A. Andryakov, A. Antonelli, M. Antonelli, et al., The tracking detector of the KLOE experiment, Nucl. Instrum. Methods, Sect. A 488 (2002) 51–73, https://doi.org/10.1016/S0168-9002(02)00514-4.
[33] M. Adinolfi, F. Ambrosino, A. Antonelli, M. Antonelli, F. Anulli, et al., The KLOE electromagnetic calorimeter, Nucl. Instrum. Methods Phys. Res., Sect. A 482 (2002) 364–386, https://doi.org/10.1016/S0168-9002(01)01502-9.
[34] M. Adinolfi, et al., The QCAL tile calorimeter of KLOE, Nucl. Instrum. Methods Phys. Res., Sect. A 483 (2002) 649–659, https://doi.org/10.1016/S0168-9002(01)01929-5.
[35] M. Adinolfi, et al., The trigger system of the KLOE experiment, Nucl. Instrum. Methods Phys. Res., Sect. A 492 (2002) 134–146, https://doi.org/10.1016/S0168-9002(02)01313-X.
[36] F. Ambrosino, et al., Data handling, reconstruction, and simulation for the KLOE experiment, Nucl. Instrum. Methods Phys. Res., Sect. A 534 (2004) 403–433, https://doi.org/10.1016/j.nima.2004.06.155, arXiv:physics/0404100.
[37] A. Gajos, Investigations of fundamental symmetries with the electron-positron systems, Ph.D. thesis, Jagiellonian University, Kraków, Poland, 2018, arXiv:1805.06009, http://koza.if.uj.edu.pl/files/40f2a1011572dd7e0c9988c54dcaecaa/1805.06009.pdf.
[38] E. Ramberg, et al., Simultaneous Measurement of K_S and K_L Decays into $\pi^+\pi^-\gamma$, Phys. Rev. Lett. 70 (1993) 2525–2528, https://doi.org/10.1103/PhysRevLett.70.2525.
[39] C. Gatti, Monte Carlo simulation for radiative kaon decays, Eur. Phys. J. C 45 (2006) 417–420, https://doi.org/10.1140/epjc/s2005-02435-2, arXiv:hep-ph/0507280.
[40] A. Hocker, et al., TMVA - toolkit for multivariate data analysis, arXiv:physics/0703039, 3 2007.
[41] A. Apostolakis, et al., A Determination of the CP violation parameter eta+- from the decay of strangeness tagged neutral kaons, Phys. Lett. B 458 (1999) 545–552, https://doi.org/10.1016/S0370-2693(99)00596-1.
[42] M. Zobov, D. Alesini, M.E. Biagini, C. Biscari, A. Bocci, et al., Test of "crab-waist" collisions at the DAΦNEΦ factory, Phys. Rev. Lett. 104 (2010)

174801, https://doi.org/10.1103/PhysRevLett.104.174801, https://link.aps.org/doi/10.1103/PhysRevLett.104.174801.
[43] C. Milardi, M.A. Preger, P. Raimondi, F. Sgamma, High luminosity interaction region design for collisions inside high field detector solenoid, J. Instrum. 7 (2012) T03002, https://doi.org/10.1088/1748-0221/7/03/T03002, arXiv:1110.3212.